JOURNAL OF GEOPHYSICAL RESEARCH, VOL. 115, A02310, doi:10.1029/2009JA014448, 2010

Ionospheric ion-acoustic enhancements by turbulent counterstreaming electron beam-plasma interaction

J. Pavan,[1] L. F. Ziebell,[1] P. H. Yoon,[2,3,4] and R. Gaelzer[5]

Received 12 May 2009; revised 16 September 2009; accepted 24 September 2009; published 12 February 2010.

[1] Ion-acoustic enhancements are investigated within the context of turbulent beam-plasma interaction processes. The analysis assumes a pair of counterstreaming electron beams interacting with the background plasma. Two-dimensional velocity space and two-dimensional wave number space are assumed for the analysis, with physical parameters that characterize typical ionospheric conditions. The solutions of the electrostatic weak turbulence theory show that the ion-acoustic wave levels are significantly enhanced when the computation is initialized with a pair of counterstreaming beams in contrast to a single beam. We suggest that this finding is highly relevant for the observed ion-acoustic enhancements in the Earth's ionosphere that are known to be correlated with auroral activity.

Citation: Pavan, J., L. F. Ziebell, P. H. Yoon, and R. Gaelzer (2010), Ionospheric ion-acoustic enhancements by turbulent counterstreaming electron beam-plasma interaction, *J. Geophys. Res.*, *115*, A02310, doi:10.1029/2009JA014448.

1. Introduction

[2] The generation mechanism for naturally enhanced ion-acoustic waves is still a matter of debate. Ever since it was realized that such signals are of geophysical nature [*Foster et al.*, 1988; *Collis et al.*, 1991], a considerable amount of data have been acquired and reported, on the basis of which the general understanding of the main characteristics associated with the enhanced ion-acoustic waves in the Earth's ionosphere has emerged.

[3] These transient signals are customarily interpreted as enhancements of ion-acoustic waves by 1–2 orders of magnitude over thermal level [*Rietveld et al.*, 1991; *Collis et al.*, 1991]. These waves travel up or down along the geomagnetic field in the Earth's ionosphere, and their intensities diminish off within $\lesssim 15°$ away from the direction parallel to B field [*Foster et al.*, 1988; *Rietveld et al.*, 1991]. Data obtained with incoherent scatter radar experiments reveal that sometimes the ion-acoustic waves can be enhanced in both directions, while at other times they are primarily enhanced in one direction only. These data show that the ionospheric ion-acoustic enhancements do not follow a strict pattern, but are quite irregular.

[4] In spite of the irregular nature associated with ion-acoustic enhancements (IAE), however, it seems to exist an overall altitude dependency of various features associated with IAE. *Foster et al.* [1988] report that the amplitude of ion-acoustic lines generally increases for increasing altitudes. According to *Rietveld et al.* [1991] the general range of altitudes for which IAE take place corresponds to ~138 to ~567 km and up. In the upper region of the IAE source region, symmetric IAE peaks are often detected, while in the lower region the upper IAE peak is preferentially enhanced. Also the gap between the two peaks seems to increase as the source altitude increases [*Buchert et al.*, 1999]. These generalizations notwithstanding, a great variability in IAE spectral features is found in time and altitude [*Rietveld et al.*, 1991].

[5] Another important characteristic concerns the occurrence of IAE and auroral activity. IAE are often observed concomitantly with field-aligned currents, red and green auroras, electron precipitation, and geomagnetic disturbance [*Foster et al.*, 1988; *Rietveld et al.*, 1991; *Collis et al.*, 1991; *Buchert et al.*, 1999]. Ion outflows also frequently accompany IAE. More recently, auroral filamentary structures have been observed in relation to IAE [*Grydeland et al.*, 2003]. In particular, comparable spatial scales were found for both auroral and IAE sources. Magnetic field-aligned structures were estimated to have perpendicular scale lengths ranging from a few hundred meters or less. Within these field-aligned structures having perpendicular density gradients, IAE of 4–5 orders above thermal level in magnitude were observed [*Grydeland et al.*, 2003]. Filamentary structures are also linked to rayed aurora. *Blixt et al.* [2005] report a positive correlation between IAE and flaming aurora. These authors also argue that the occurrence of active rayed aurora is a sufficient condition for the occurrence of IAE, although it may not be a necessary condition.

[6] A number of theories have been proposed for IAE. *Bythrow et al.* [1984] suggest that the ion-acoustic mode destabilization by streaming electrons may be the source mechanism. Their reasoning is based upon the detection

[1]Instituto de Física, Universidade Federal do Rio Grande do Sul, Porto Alegre, Brazil.
[2]Massachusetts Technological Laboratory, Inc., Belmont, Massachusetts, USA.
[3]Institute for Physical Science and Technology, University of Maryland College Park, College Park, Maryland, USA.
[4]School of Space Research, Kyung Hee University, Yongin, South Korea.
[5]Instituto de Física e Matemática, Universidade Federal de Pelotas, Pelotas, Brazil.

0148-0227/10/2009JA014448$09.00

of intense Birkeland currents by HILAT satellite showing related electron fluxes which were above the threshold for the destabilization. *Collis et al.* [1991] put forth the idea that relative drift between electrons and ions may lead to the ion-acoustic-type instability. The estimated field-aligned currents based upon the relative ion-to-electron drift, however, turned out to be too high (~mA m^{-2}) in comparison with typical measured values (~μA m^{-2}). Besides, their approach cannot explain two simultaneous peaks in IAE. In their model for electric field formation in the ionosphere, *Rietveld et al.* [1991] argue that field-aligned thermal electron drifts, rather than bump-on-tail-like drifts, are ultimately responsible for destabilizing ion-acoustic waves.

[7] *Wahlund et al.* [1992], on the other hand, consider ion-ion two-stream instability as the cause of IAE. While their model may provide an essential explanation for the observed double spectral peaks, and may be in agreement with observed occurrence conditions for typical topside ionospheric parameters, their analysis is still limited to linear theory.

[8] *Forme and Fontaine* [1999] present a possible explanation for the origin of ion outflows accompanying IAE. They estimate the value of the plasma parameters inside the source of IAE. They argue that strong electron temperature gradients associated with the ion-acoustic turbulence in the source region lead to enhanced ambipolar electric field, which may account for the observed ion outflows.

[9] The first nonlinear theory of IAE was carried out by *Forme* [1993, 1999] who employed a weak turbulence theory in order to explain the generation mechanism of IAE. The author successfully obtained solutions that correspond to ion-acoustic enhancements either in one direction only or in both directions. In this one-dimensional (1-D) study, the author neglects nonlinear wave-particle interactions and spontaneous thermal effects. More recently, a 1-D weak turbulence approach has been utilized to study the decay of beam-generated Langmuir waves and the enhancement of ion-acoustic waves in the ionosphere [*Kontar and Pécseli*, 2005].

[10] The above brief account covers but a few efforts to explain IAE. The reader is referred to *Shulthess and St. Maurice* [2001] for a comprehensive review. The present analysis, which follows the weak turbulence approach, is yet another contribution to the theory of IAE. Unlike the previous effort, our theory takes into account spontaneous and induced processes, thus incorporating the balance between the two processes. Our formalism includes quasilinear (linear wave-particle), nonlinear wave-wave (three-wave decay), as well as nonlinear wave-particle (scattering) interaction processes. Moreover, we obtain numerical solutions in two-dimensional (2-D) velocity and wave number spaces.

[11] In the present paper we focus on the influence of the counterstreaming electron beams, a feature that was not properly taken into account hitherto. While a similar counterstreaming electron beam-plasma interaction problem has been investigated by us in a recent work [*Pavan et al.*, 2009], the context thereof as well as the physical parameters are rather different from the present discussion. *Pavan et al.*'s paper was motivated by solar wind application, and the choice of input parameters was made accordingly. In the present paper, we revisit the counterstreaming beam-plasma interaction problem from the standpoint of ionospheric application and with physical parameters appropriate for IAE generation problem. The IAE are observed at the high ionospheric region, where the ratio electron plasma frequency divided by electron cyclotron frequency is around 2, or larger. This numerical ratio and also the field-aligned characteristics of the phenomena involved, indicate that an unmagnetized theory can be a reasonable approximation. In fact, the unmagnetized approach has been utilized in previous analyses of the IAE found in the literature.

[12] The paper is organized as follows: In section 2, we briefly discuss the basic theoretical formalism. Section 3 presents the numerical analysis. Section 4 pertains to the discussion and comparison of numerical results against the observation. Finally, we summarize and conclude the present work in section 5.

2. Theoretical Formulation and Numerical Setup

[13] The wave kinetic equations for Langmuir (L) and ion-acoustic (S) waves that support quasilinear process as well as nonlinear decay and scattering processes are given in terms of the spectral wave energy density, $I_{\mathbf{k}}^{\sigma L}(t) = \langle E_L^{\sigma 2}(\mathbf{k}, t)\rangle$ and $I_{\mathbf{k}}^{\sigma S}(t) = \langle E_S^{\sigma 2}(\mathbf{k}, t)\rangle$, where $E_L^{\sigma}(\mathbf{k}, t)$ and $E_S^{\sigma}(\mathbf{k}, t)$ stand for the spectral electric field components associated with L and S waves, respectively, and where $\sigma = \pm 1$ stands for the sign of wave phase velocity. The wave kinetic equations for these waves are given in a recently published paper by the present group of authors [*Ziebell et al.*, 2008]. For the sake of completeness, the equations are repeated here. The nonlinear wave kinetic equations for L and S modes are given, respectively, by

$$\begin{aligned}\frac{\partial I_{\mathbf{k}}^{\sigma L}}{\partial t} &= \sigma\omega_{\mathbf{k}}^{L}\frac{\pi\omega_{pe}^{2}}{k^{2}}\int d\mathbf{v}\,\delta\left(\sigma\omega_{\mathbf{k}}^{L}-\mathbf{k}\cdot\mathbf{v}\right)\cdot\left(\frac{ne^{2}}{\pi\sigma\omega_{\mathbf{k}}^{L}}F_{e}+I_{\mathbf{k}}^{\sigma L}\,\mathbf{k}\cdot\frac{\partial F_{e}}{\partial\mathbf{v}}\right)\\ &+\sum_{\sigma',\sigma''=\pm1}\sigma\omega_{\mathbf{k}}^{L}\int d\mathbf{k}'\,V_{\mathbf{k},\mathbf{k}'}^{L}\cdot\delta\left(\sigma\omega_{\mathbf{k}}^{L}-\sigma'\omega_{\mathbf{k}'}^{L}-\sigma''\omega_{\mathbf{k}-\mathbf{k}'}^{S}\right)\\ &\times\left(\sigma\omega_{\mathbf{k}}^{L}I_{\mathbf{k}'}^{\sigma' L}\frac{I_{\mathbf{k}-\mathbf{k}'}^{\sigma'' S}}{\mu_{\mathbf{k}-\mathbf{k}'}}-\sigma''\omega_{\mathbf{k}-\mathbf{k}'}^{L}I_{\mathbf{k}}^{\sigma L}I_{\mathbf{k}'}^{\sigma' L}-\sigma'\omega_{\mathbf{k}'}^{L}I_{\mathbf{k}}^{\sigma L}\frac{I_{\mathbf{k}-\mathbf{k}'}^{\sigma'' S}}{\mu_{\mathbf{k}-\mathbf{k}'}}\right)\\ &-\sigma\omega_{\mathbf{k}}^{L}\sum_{\sigma'=\pm1}\int d\mathbf{k}'\int d\mathbf{v}\,U_{\mathbf{k},\mathbf{k}'}\\ &\times\delta\left[\sigma\omega_{\mathbf{k}}^{L}-\sigma'\omega_{\mathbf{k}'}^{L}-(\mathbf{k}-\mathbf{k}')\cdot\mathbf{v}\right]\\ &\times\left[\frac{ne^{2}}{\pi\omega_{pe}^{2}}\left(\sigma'\omega_{\mathbf{k}'}^{L}I_{\mathbf{k}}^{\sigma L}-\sigma\omega_{\mathbf{k}}^{L}I_{\mathbf{k}'}^{\sigma' L}\right)F_{i}\right.\\ &\left.-\frac{m_{e}}{m_{i}}I_{\mathbf{k}'}^{\sigma' L}I_{\mathbf{k}}^{\sigma L}(\mathbf{k}-\mathbf{k}')\cdot\frac{\partial F_{i}}{\partial\mathbf{v}}\right],\end{aligned} \tag{1}$$

$$\begin{aligned}\frac{\partial}{\partial t}\frac{I_{\mathbf{k}}^{\sigma S}}{\mu_{\mathbf{k}}} &= \mu_{\mathbf{k}}\sigma\omega_{\mathbf{k}}^{L}\frac{\pi\omega_{pe}^{2}}{k^{2}}\int d\mathbf{v}\,\delta\left(\sigma\omega_{\mathbf{k}}^{S}-\mathbf{k}\cdot\mathbf{v}\right)\\ &\times\left[\frac{ne^{2}}{\pi\sigma\omega_{\mathbf{k}}^{L}}(F_{e}+F_{i})+\frac{I_{\mathbf{k}}^{\sigma S}}{\mu_{\mathbf{k}}}\,\mathbf{k}\cdot\frac{\partial}{\partial\mathbf{v}}\left(F_{e}+\frac{m_{e}}{m_{i}}F_{i}\right)\right]\\ &+\frac{1}{2}\sum_{\sigma',\sigma''=\pm1}\sigma\omega_{\mathbf{k}}^{L}\int d\mathbf{k}'\,V_{\mathbf{k}',\mathbf{k}-\mathbf{k}'}^{S}\\ &\times\delta\left(\sigma\omega_{\mathbf{k}}^{S}-\sigma'\omega_{\mathbf{k}'}^{L}-\sigma''\omega_{\mathbf{k}-\mathbf{k}'}^{L}\right)\\ &\times\left(\sigma\omega_{\mathbf{k}}^{L}I_{\mathbf{k}'}^{\sigma' L}I_{\mathbf{k}-\mathbf{k}'}^{\sigma'' L}-\sigma'\omega_{\mathbf{k}'}^{L}I_{\mathbf{k}-\mathbf{k}'}^{\sigma'' L}\frac{I_{\mathbf{k}}^{\sigma S}}{\mu_{\mathbf{k}}}-\sigma''\omega_{\mathbf{k}-\mathbf{k}'}^{L}I_{\mathbf{k}'}^{\sigma' L}\frac{I_{\mathbf{k}}^{\sigma S}}{\mu_{\mathbf{k}}}\right),\end{aligned} \tag{2}$$

where

$$V^L_{\mathbf{k},\mathbf{k}'} = \frac{\pi e^2}{2T_e^2}\frac{\mu_{\mathbf{k}-\mathbf{k}'}\,(\mathbf{k}\cdot\mathbf{k}')^2}{k^2k'^2|\mathbf{k}-\mathbf{k}'|^2},$$
$$V^S_{\mathbf{k},\mathbf{k}-\mathbf{k}'} = \frac{\pi e^2}{2T_e^2}\frac{\mu_{\mathbf{k}}\,[\mathbf{k}'\cdot(\mathbf{k}-\mathbf{k}')]^2}{k^2k'^2|\mathbf{k}-\mathbf{k}'|^2},$$
$$U_{\mathbf{k},\mathbf{k}'} = \frac{\pi e^2}{m_e^2\omega_{pe}^2}\frac{(\mathbf{k}\cdot\mathbf{k}')^2}{k^2\,k'^2}.$$

[14] The dispersion relations for L and S modes are well known:

$$\omega^L_{\mathbf{k}} = \omega_{pe}\left(1+\frac{3}{2}\,k^2\lambda_{De}^2\right),$$
$$\omega^S_{\mathbf{k}} = \omega_{pe}\,\frac{k\lambda_{De}}{(1+k^2\lambda_{De}^2)^{1/2}}\left(\frac{m_e}{m_i}\right)^{\frac{1}{2}}\left(1+\frac{3T_i}{T_e}\right)^{\frac{1}{2}},$$

where λ_{De} is the electron Debye length, T_e is the electron temperature associated with the dense core electrons, and T_i the ion temperature. In (1) and (2) we have also introduced a quantity

$$\mu_{\mathbf{k}} = k^3\lambda_{De}^3\left(\frac{m_e}{m_i}\right)^{\frac{1}{2}}\left(1+\frac{3T_i}{T_e}\right)^{\frac{1}{2}}.$$

[15] The first terms on the right-hand sides of (1) and (2) describe the spontaneous and induced emission process which together constitute quasilinear (or linear wave-particle interaction) processes. The second terms contain the wave energy and momentum conservation condition, $\delta(\sigma\omega^L_{\mathbf{k}} - \sigma'\omega^L_{\mathbf{k}'} - \sigma''\omega^S_{\mathbf{k}-\mathbf{k}'})$ for L mode and a similar three-wave resonance condition for S mode, and they describe the three-wave decay (nonlinear wave-wave interaction) processes. The third term in (1) contains the nonlinear wave-particle resonance condition $\delta[\sigma\omega^L_{\mathbf{k}} - \sigma'\omega^L_{\mathbf{k}'} - (\mathbf{k}-\mathbf{k}')\cdot\mathbf{v}]$, and it depicts the scattering of L waves by thermal ions. We have neglected the scattering effects for (2) that governs the evolution of S waves, since the scattering processes involving S waves are extremely slow processes.

[16] The electron particle kinetic equation is given by the Fokker–Planck form,

$$\frac{\partial F_e(\mathbf{v})}{\partial t} = \frac{\partial}{\partial v_i}\left[A_i(\mathbf{v})\,F_e(\mathbf{v}) + D_{ij}(\mathbf{v})\,\frac{\partial F_e(\mathbf{v})}{\partial v_j}\right],$$
$$A_i(\mathbf{v}) = \frac{e^2}{4\pi m_e}\int d\mathbf{k}\,\frac{k_i}{k^2}\sum_{\sigma=\pm1}\sigma\omega^L_{\mathbf{k}}\,\delta(\sigma\omega^L_{\mathbf{k}} - \mathbf{k}\cdot\mathbf{v}), \qquad (3)$$
$$D_{ij}(\mathbf{v}) = \frac{\pi e^2}{m_e^2}\int d\mathbf{k}\,\frac{k_i\,k_j}{k^2}\sum_{\sigma=\pm1}\delta(\sigma\omega^L_{\mathbf{k}} - \mathbf{k}\cdot\mathbf{v})\,I^{\sigma L}_{\mathbf{k}}.$$

The term with coefficient A_i describes effects owing to spontaneous thermal fluctuations, and the term with coefficient D_{ij} governs the velocity space diffusion process. Ions are treated as quasistationary. In 2-D, the ion distribution is given by $F_i = (m_i/2\pi T_i)\exp(-m_iv^2/2T_i)$, where T_i and m_i are the ion temperature and the proton mass, respectively.

[17] The initial electron distribution corresponds to a combined Maxwellian background plus tenuous components of drifting Gaussian beam populations. In 2-D, it is given by

$$F_e(t=0) = \frac{1-n_b/n-n_f/n}{\pi v_{te}^2}\exp\left[-\frac{v_\perp^2}{v_{te}^2} - \frac{(v_\parallel - v_e)^2}{v_{te}^2}\right] + \frac{n_b/n}{\pi v_{tb}^2}\exp\left[-\frac{v_\perp^2}{v_{tb}^2} - \frac{(v_\parallel + v_b)^2}{v_{tb}^2}\right] + \frac{n_f/n}{\pi v_{tf}^2}\exp\left[-\frac{v_\perp^2}{v_{tf}^2} - \frac{(v_\parallel - v_f)^2}{v_{tf}^2}\right].$$

Here $v_{te}^2 = 2T_e/m_e$, $v_{tb}^2 = 2T_b/m_e$, and $v_{tf}^2 = 2T_f/m_e$ correspond to squares of thermal speeds associated with the core electrons, backward and forward propagating beam electrons, respectively, and v_e, v_b, and v_f are the drift speeds of the background, backward and forward traveling beams, respectively. We have imposed the average drift velocity $v_e = (n_bv_b - n_fv_f)/(n - n_b - n_f)$ for the core electrons, so that zero net drift velocity for the entire electron distribution is guaranteed.

[18] Intense ionospheric paired currents associated to IAE were observed with densities 10 to 20 μA m^{-2} [*Burke et al.*, 1983]. Very intense small-scale features superimposed on large-scale Birkeland currents were also observed [*Bythrow et al.*, 1984]. These show that modeling the source of IAE by counterstreaming electron beams (that is, small-scale current flowing both ways) is not unreasonable.

[19] The source of IAE generation may also coincide with two adjacent regions carrying intense currents in opposite directions, up and down the field lines. Electrons moving in both directions along the field were observed in the transition altitude region possibly associate to electric field reversal [*Rietveld et al.*, 1991].

[20] Furthermore, geomagnetic mirror and back-scattered ionospheric electrons may also lead to the counterstreaming beams situation [*Forme*, 1993]. These beams may also be due to the differences in intensities of low- and high-frequency fields in ionosphere [*Block and Fälthammar*, 1990; *McFadden et al.*, 1999]. In short, the present model of counterstreaming Gaussian electron beams interacting with the core background plasma is a reasonable approach.

[21] We initialize the wave intensities by balancing the spontaneous and induced emissions, taking into account the background populations:

$$I^{\sigma L}_{\mathbf{k}}(0) = \frac{T_e}{4\pi^2}\frac{1}{1+3k^2\lambda_{De}^2},$$
$$I^{\sigma S}_{\mathbf{k}}(0) = \frac{T_e}{4\pi^2}\,k^2\lambda_{De}^2\sqrt{\frac{1+k^2\lambda_{De}^2}{1+3k^2\lambda_{De}^2}} \times \frac{\int d\mathbf{v}\;\delta(\sigma\omega^S_{\mathbf{k}} - \mathbf{k}\cdot\mathbf{v})\,(F_e+F_i)}{\int d\mathbf{v}\;\delta(\sigma\omega^S_{\mathbf{k}} - \mathbf{k}\cdot\mathbf{v})[F_e + (T_e/T_i)\,F_i]}.$$

[22] For the numerical solution, we have rewritten the kinetic equations (1)–(3) in terms of normalized quantities, i.e., $I^{\sigma L,S}_{\mathbf{k}}$ multiplied by $g/(2^{7/2}m_ev_{te}^2)$, where $g = 1/n\lambda_{De}^3$ is the plasma parameter, and $F_{i,e}$ multiplied by $v_{te}{}^{\mathcal{D}}$, where $\mathcal{D}$

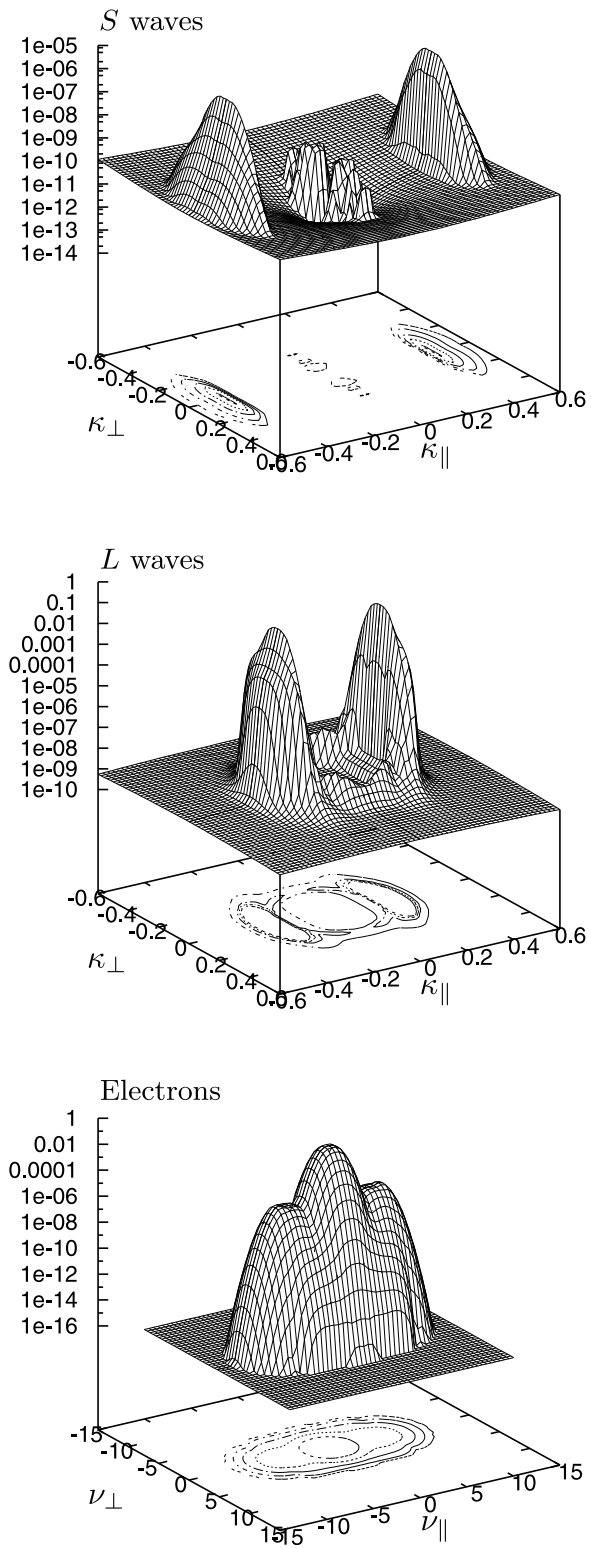

Figure 1. Three-dimensional mesh plots of (top) S and (middle) L spectra and (bottom) electron distribution for $\eta_b = \eta_f = 2$, $\nu_b = \nu_f = 5$, and $g = 10^{-6}$ at $\tau = 5000$. Figure 1 (top) and (middle) show the normalized wave intensities $\mathcal{E}^{\sigma S}_{\mathbf{k}} = I^{\sigma S}_{\mathbf{k}} g/(2^{7/2} m_e v^2_{te})$ and $\mathcal{E}^{\sigma L}_{\mathbf{k}} = I^{\sigma L}_{\mathbf{k}} g/(2^{7/2} m_e v^2_{te})$, respectively, and Figure 1 (bottom) shows $v^2_{te} F_e$.

is the dimensionality considered. In the normalized form, the plasma parameter g appears explicitly multiplying the terms related to the spontaneous emission and scattering processes. We solved the coupled particle (electron) and wave kinetic equations in 2-D wave number space and 2-D velocity space (i.e., $\mathcal{D} = 2$) numerically by employing the Runge–Kutta procedure for the wave equations, while the particle kinetic equation is solved by implicit method in alternate direction (the alternating direction implicit (ADI) method). We employed 61 × 61 grids for $\kappa_\perp$ and $\kappa_\parallel$, with $0 < \kappa_\perp < 0.6$ and $0 < \kappa_\parallel < 0.6$, where $\kappa_\perp = k_\perp v_{te}/\omega_{pe}$ and $\kappa_\parallel = k_\parallel v_{te}/\omega_{pe}$. For the velocities, we used 51 × 101 grids for $\nu_\perp$ and $\nu_\parallel$, covering the velocity range $0 < \nu_\perp < 12$ and $-12 < \nu_\parallel < 12$, where $\nu_\perp = v_\perp/v_{te}$ and $\nu_\parallel = v_\parallel/v_{te}$. The present scheme excludes exactly zero $\kappa_\parallel$, but we interpolate physical quantities to $\kappa_\parallel = 0$. In the subsequent numerical solutions we assume electron-to-ion temperature ratio $T_e/T_i = 3$, which is typical of the topside ionosphere [*Rietveld et al.*, 1991; *Collis et al.*, 1991; *Forme*, 1999; *Forme and Fontaine*, 1999]. Equal beam-to-background temperatures are assumed, $T_b/T_e = T_f/T_e = 1.0$.

[23] We define the beam-to-total density ratios $\overline{\eta}_b = n_b/n$ and $\overline{\eta}_f = n_f/n$, respectively, and introduce another quantity, $\eta_{b,f}$ where $\eta_{b,f} = \overline{\eta}_{b,f} \times 10^4$. The normalized time is given by $\tau = \omega_{pe} t$, the normalized backward and forward beam velocities are given by $\nu_{b,f} = v_{b,f}/v_{te}$, and $n - n_b - n_f = n_e \sim n$, where n_e stands for the background electron density.

3. Results

[24] Figure 1 shows a typical output from solving equations (1)–(3) by numerical means. Figure 1 was obtained for $\eta_b = \eta_f = 2$. The result shown in Figure 1 is a snapshot of the wave-particle system at $\tau = 5000$. Since our main concern is on ion-acoustic waves, let us focus on the S waves first (Figure 1 (top)). According to Figure 1, S wave intensity in the nonlinear stage ($\tau = 5000$) is characterized by a pair of peaks for large $|k_\parallel|$ range that are significantly enhanced over thermal level. There also exists a third and weaker intensity peak near $k \sim 0$. The outer peaks have parallel wave numbers that are twice that of the Langmuir waves, $k^S \sim 2k^L$, as expected from nonlinear decay instability theory.

[25] The peak near $k \sim 0$ is originated by the process of spontaneous decay. The point is that the spontaneous decay term in equation (2) is proportional to $I^{\sigma' L}_{\mathbf{k}'} I^{\sigma'' L}_{\mathbf{k}-\mathbf{k}'}$. The Langmuir waves appearing in this term feature peaks created by the quasilinear process. Because of the resonance condition and to the narrow beam, these peaks occur at wave numbers close to the inverse of the beam velocity. That is, $I^{\sigma' L}_{\mathbf{k}'}$ is maximum at $|\mathbf{k}'| \simeq 1/v_{f,b}$ and $I^{\sigma'' L}_{\mathbf{k}-\mathbf{k}'}$ is maximum at $|\mathbf{k} - \mathbf{k}'| \simeq 1/v_{f,b}$. In order to satisfy simultaneously these conditions it is necessary that $\mathbf{k} \simeq 2\mathbf{k}'$, or $\mathbf{k} \simeq \mathbf{0}$. On the other hand, since $\omega^S \ll \omega^L$, the resonance condition for the three-wave decay process can be approximated by $\omega^L_{\mathbf{k}'} \simeq \omega^L_{\mathbf{k}-\mathbf{k}'}$, leading to the conclusion that $k'^2 \simeq |\mathbf{k} - \mathbf{k}'|^2$. The values $\mathbf{k} \simeq 0$ and $\mathbf{k} \simeq 2\mathbf{k}'$, which lead to the maximum of the product $I^{\sigma' L}_{\mathbf{k}'} I^{\sigma'' L}_{\mathbf{k}-\mathbf{k}'}$, clearly satisfy the resonance condition. Another aspect to be considered is that the efficiency of the three-wave process also depends on the *transition coefficient* which multiplies the product of the L wave

amplitudes. Equation (2) shows that this coefficient contains

$$k^6 \frac{|\mathbf{k}' \cdot (\mathbf{k} - \mathbf{k}')|^2}{k^2 k'^2 |\mathbf{k} - \mathbf{k}'|^2},$$

which can be written as $k^4 \cos^2\theta$, where θ is the angle between $\mathbf{k}'$ and $\mathbf{k} - \mathbf{k}'$. The expression shows that

$$\cos^2\theta = \frac{|\mathbf{k}' \cdot (\mathbf{k} - \mathbf{k}')|^2}{k'^2 |\mathbf{k} - \mathbf{k}'|^2}.$$

[26] It is easy to see that the cases $\mathbf{k} = 0$ and $\mathbf{k} = 2\mathbf{k}'$ maximize the value of $\cos^2\theta$. Considering the product of the transition coefficient and of the quantity $I_{\mathbf{k}'}^{\sigma' L} I_{\mathbf{k}-\mathbf{k}'}^{\sigma'' L}$, it is seen that the three-wave decay term will be maximum for $\mathbf{k} \simeq 2\mathbf{k}'$ and for $\mathbf{k} \simeq 0$, although not exactly at $\mathbf{k} = 0$. Since the spontaneous decay term is at the right-hand side of an equation for the time evolution of $I_{\mathbf{k}}^{\sigma S}$, one is led to the conclusion that the S waves grow at these wavelengths. These considerations about the growth of S waves for $\mathbf{k} \simeq 2\mathbf{k}'$ and for $\mathbf{k} \simeq \mathbf{0}$ are also validated by earlier results obtained by an approximated analytical treatment of the three-wave decay of beam-driven Langmuir waves into ion-acoustic waves [*Edney and Robinson*, 2001].

[27] Langmuir (L) waves (Figure 1 (middle)) are primarily driven by the counterstreaming beam-plasma instability in the linear stage and exponentially grow from the initial thermal level. However, in the late nonlinear stage ($\tau = 5000$) L mode spectrum evolves into a ring spectrum in 2-D wave number space as a result of nonlinear interaction processes.

[28] The electron distribution (Figure 1 (bottom)) forms a quasilinear plateau in both forward- and backward directions by the time the system has evolved to $\tau = 5000$. In addition to the plateau formation, the electron population in the tail region is actually slightly heated to superthermal energies. The tail formation is the result of L waves being redistributed in wave number space toward smaller parallel wave number range by nonlinear mode-coupling effects. The low $k_\parallel$ Langmuir waves are then subsequently absorbed by electrons with high $v_\parallel$, and thus the superthermal population is produced.

[29] Figure 2 shows the time evolution of S waves in 1-D reduced $k_\parallel$ space. Figure 2 is for $\eta_b = \eta_f = 10$, and the 1-D spectra show the quantity $\mathcal{E}_\parallel^S$, obtained by integration of the normalized S wave spectrum over $k_\perp$. Figure 2 shows that the peak intensity grows from thermal level value to a significant level at $\tau = 1000$, reaches maximum at $\tau = 2000$, and starts to decrease thereafter. At $\tau = 5000$, S waves have undergone a substantial reduction in intensity. Nevertheless, the height of the S wave peaks at this time is still well above the thermal level. Transient behavior associated with S mode turbulence as seen by Figure 2 may thus be highly relevant to the prominent transient feature usually accompanying the observed IAE in the ionosphere.

[30] Figures 1 and 2 were generated for plasma parameter $g = 1/n_e \lambda_{De}^3 = 10^{-6}$ that is consistent with typical ionospheric parameters $T_e \sim 6000$ K and $n_e \sim 10^{11}$ m^{-3} [*Rietveld et al.*, 1991; *Cabrit et al.*, 1996; *Forme and Fontaine*, 1999]. The plasma parameter affects the spontaneous thermal effects; the higher the value of g, the more important are the roles of spontaneous emission and scattering. Figure 3 shows the effects of varying the g parameter by plotting the reduced 1-D S wave spectra versus $k_\parallel$, for various values of g ranging from 10^{-2} to 10^{-6}, at a time nearly corresponding to the maximum of the S wave enhancements. For decreasing g, the thermal level goes down accordingly, but the twin peaks in the S mode actually increase sharply as a function of g. The dependence of the ion-acoustic enhancements on g, which is displayed in Figure 3, deserves further comments. For instance, an increase of g can be obtained by reduction of the plasma density, for fixed electron temperature. However, if the density is changed, the ratios $n_{f,b}/n$ are also changed, unless the beam densities are changed as well. Moreover, since the ion-acoustic enhancements occur at $k^S \sim 2k^L \sim (\omega_{pe}/v_{b,f})$, they appear at different values of wave number, for different plasma densities. This difference disappears with the use of the normalized wave numbers, $\kappa_\parallel$ and $\kappa_\perp$. Another form to vary g is by variation of the electron temperature. Of course, a variation of T_e would lead to modification of ratios like $v_{f,b}/v_{te}$, unless other quantities are changed along with the electron temperature. Therefore, the results depicted in Figure 3 for increasing g can be regarded as the result of either decreasing plasma density with fixed electron temperature, or of decreasing electron temperature with fixed plasma density, with other parameters changed conveniently in order to keep fixed the normalized quantities utilized as parameters. The bottomline is that, because of the use of normalized quantities, g can be varied as an independent parameter, as in the case displayed in Figure 3. The results obtained show that the IAE are strongly enhanced relative to the thermal level, for small values of g, as is the case for ionospheric parameters. Since g appears in the equations multiplying the terms connected with spontaneous emission or scattering, the meaning of these results is that the IAE become more significant when the effect of spontaneous emission and scattering is decreased. This finding is in contrast with the dependence on g displayed by another phenomena recently investigated with use of weak turbulence theory, which is the generation of superthermal electron tails, since it has been shown that these tails are generated only for sufficiently high values of g [*Yoon et al.*, 2006].

[31] Figure 4 shows 1-D S waves spectra for different combinations of back and forward beam densities. All distinct sets add up to the same total beam densities, $\overline{\eta}_b + \overline{\eta}_f = 10^{-3}$. Results were obtained for ($\eta_b = 5$, $\eta_f = 5$), ($\eta_b = 4$, $\eta_f = 6$), ($\eta_b = 3$, $\eta_f = 7$), ($\eta_b = 2$, $\eta_f = 8$), ($\eta_b = 1$, $\eta_f = 9$), and ($\eta_b = 0$, $\eta_f = 10$), for times nearly corresponding to the maximum of the S wave enhancements. The most noteworthy feature associated with Figure 4 is the high increase of turbulence intensity in the case of symmetrical counterstreaming beams in comparison to the single-beam system; while a single beam leads to an increase of ~1 order of magnitude over the thermal level, the symmetrical beams exceed over ~4 orders of magnitude over the thermal level. The transition from the single beam to the symmetrical system is not monotonic. There is sudden increase of wave intensity going from ($\eta_b = 0$, $\eta_f = 10$) to ($\eta_b = 2$, $\eta_f = 8$), but further increase is very gradual thereafter. Note that for ($\eta_b = 2$, $\eta_f = 8$) the intensity is enhanced by nearly ~3 orders of magnitude over the thermal

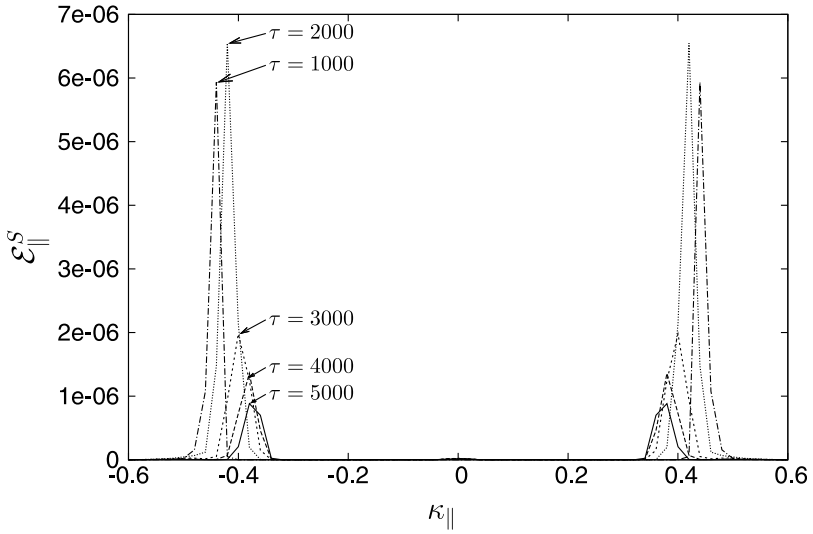

Figure 2. Time evolution of reduced ion-acoustic turbulence intensity versus normalized parallel wave number for $\eta_b = \eta_f = 10$, $\nu_b = \nu_f = 5$, and $g = 10^{-6}$.

level. This means that even a "mildly" symmetrical beams system is able in producing strong enhancements of *S* waves.

[32] Figure 5 shows *S* wave spectra for different combinations of the beams drifts ν_b and ν_f, at times nearly corresponding to the maximum of the *S* wave enhancements. Results are obtained for symmetrical beams, $\nu_b = \nu_f = 5$, and nonsymmetrical beams, $\nu_b = 6$, $\nu_f = 5$ and $\nu_b = 7$, $\nu_f = 5$. It is highly interesting to note that the wave intensity is enhanced for decreasing ν_b (for fixed ν_f), although decreasing ν_b means less free energy. This finding shows that the enhanced *S* mode turbulence is directly associated with the counterstreaming beams being exactly symmetrical in both directions. The explanation is based on the fact that the Langmuir peaks occur at wave number close to the inverse of the beam velocities. The forward beam originates a *L* wave peak for $|\mathbf{k}| = |\mathbf{k_f}| \sim 1/v_f$, and the backward beam originates in the opposite sense a *L* wave peak for $|\mathbf{k}| = |\mathbf{k_b}| \sim 1/v_b$. Afterwards, in a slower time scale, three-wave decay and scattering produce secondary peaks, respectively, at $\mathbf{k} \simeq -\mathbf{k_f}$ and $\mathbf{k} \simeq -\mathbf{k_b}$. If v_b is close to v_f, $\mathbf{k_b} \simeq -\mathbf{k_f}$. That is, the nonlinear processes reinforce the peaks produced by the quasilinear process, and as a consequence the *S* waves caused by the spontaneous decay term are enhanced.

[33] Figure 6 presents 2-D spectra for *S* waves for different combinations of beam densities, namely, $\eta_b = \eta_f = 2$, $\eta_b = \eta_f = 6$, and $\eta_b = \eta_f = 10$, at times nearly corresponding to the maximum of the *S* wave enhancements. Contour lines are drawn starting at 2×10^{-10}, nearly the thermal level for the outermost peaks, and new contours are set at each order of magnitude higher. Diagonal lines are superposed in order to aid the readers assess the angular extents associated with enhanced *S* waves. Note that the wave spectra spread out in

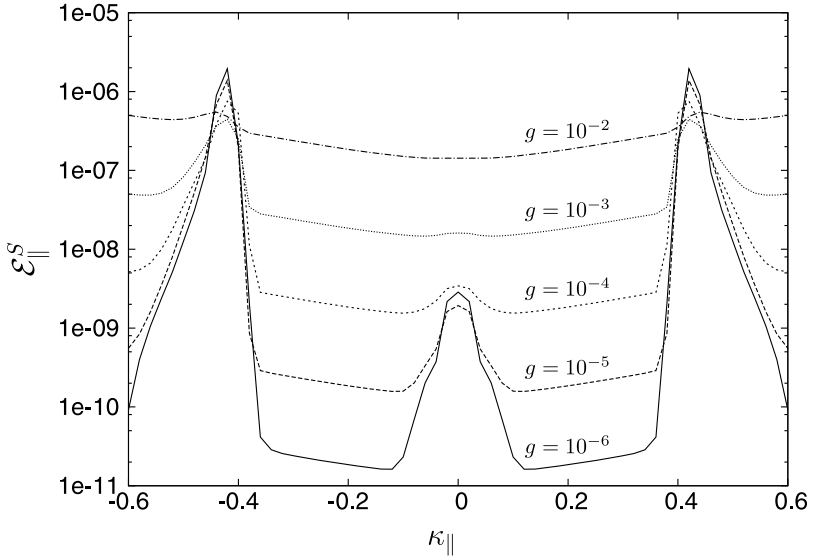

Figure 3. Reduced ion-acoustic turbulence intensity versus normalized parallel wave number for different values of plasma parameter *g* for $\eta_b = \eta_f = 5$ and $\nu_b = \nu_f = 5$ in log scale for intensity. Here $g = 10^{-2}$, $\tau = 1500$; $g = 10^{-3}$, $\tau = 2000$; $g = 10^{-4}$, $\tau = 2500$; $g = 10^{-5}$, $\tau = 2500$; and $g = 10^{-6}$, $\tau = 3000$ are shown.

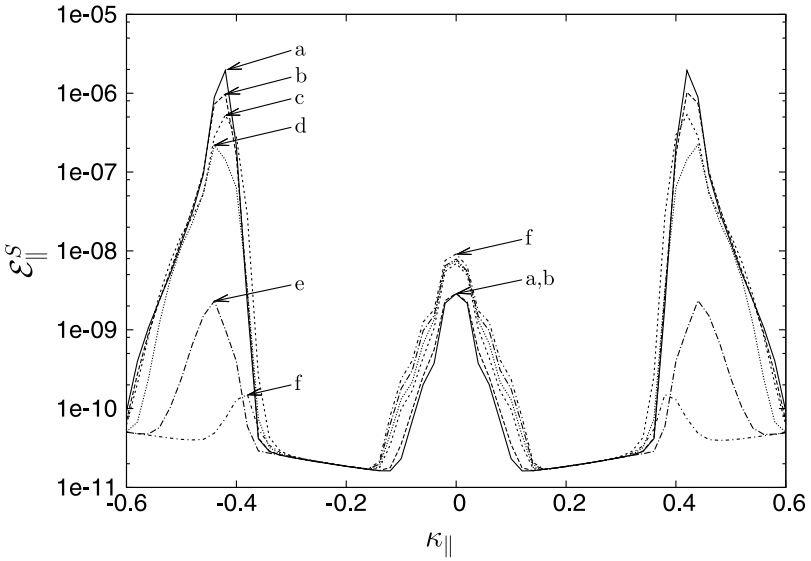

Figure 4. Evolution from a single-beam system to a system containing fully symmetrical counterstreaming beams: $\eta_b = 5$, $\eta_f = 5$, $\tau = 3000$ (curve a); $\eta_b = 4$, $\eta_f = 6$, $\tau = 3000$ (curve b); $\eta_b = 3$, $\eta_f = 7$, $\tau = 4000$ (curve c); $\eta_b = 2$, $\eta_f = 8$, $\tau = 4500$ (curve d); $\eta_b = 1$, $\eta_f = 9$, $\tau = 5000$ (curve e); and $\eta_b = 0$, $\eta_f = 10$, $\tau = 5000$ (curve f). In all cases, $\nu_b = \nu_f = 5$ and $g = 10^{-6}$.

both the perpendicular and parallel direction as density increases, leading to wider angular extents for higher density. This occurs because the ion-acoustic enhancements are produced by nonlinear processes which depend on the intensity of the forward and backward Langmuir peaks, which are fueled by the electron beams. The higher the density of the beams, the more efficient and faster are the nonlinear processes. Particularly, for higher density beams, broader and taller Langmuir peaks are generated, which further decay over a larger region of the wave number space, in comparison with the cases of less dense beams.

[34] Figure 7 is similar to Figure 6 except that now we vary the beams drifts; $\nu_b = \nu_f = 5.5$, $\nu_b = \nu_f = 6$, and $\nu_b = \nu_f = 6.5$. As in Figure 7, contour lines are drawn starting at 2×10^{-10}, nearly the thermal level for the outermost peaks, and new contours are set at each order of magnitude higher. Note that angular spread increases for higher drift speeds as diagonal lines indicate. This is largely owing to that fact that higher drift speeds causes the S waves spectrum to shift toward lower $k_\parallel$ while maintaining roughly the same width in $k_\perp$ direction. The reason for inward shift

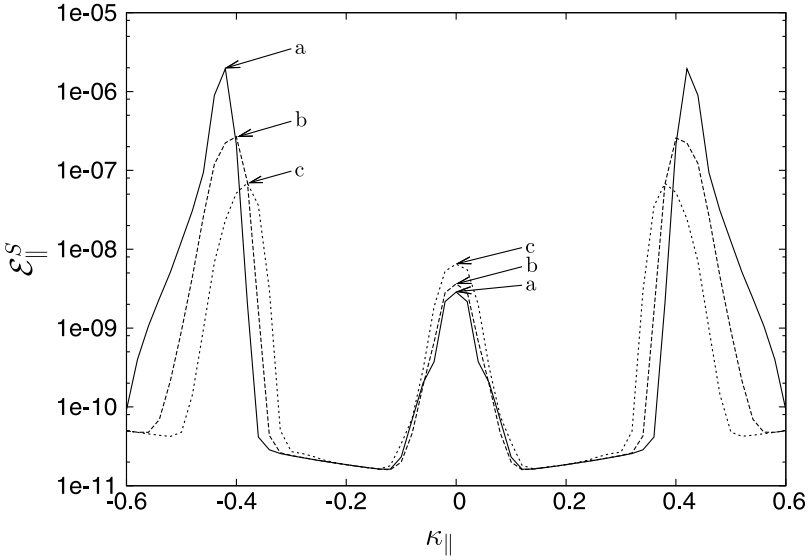

Figure 5. Ion-acoustic enhancements for different beam speeds: $\nu_b = 5$, $\nu_f = 5$, $\tau = 3000$ (curve a); $\nu_b = 6$, $\nu_f = 5$, $\tau = 3000$ (curve b); and $\nu_b = 7$, $\nu_f = 5$, $\tau = 4000$ (curve c). In the three cases, $\eta_b = \eta_f = 5$ and $g = 10^{-6}$.

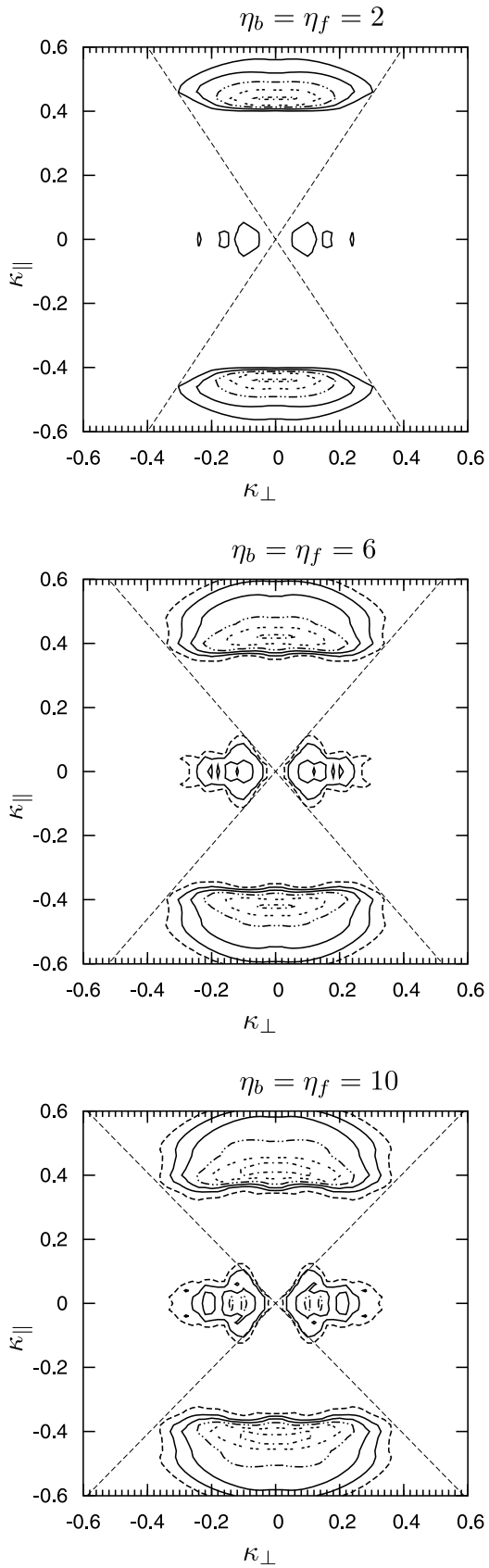

of S mode spectrum along $k_\parallel$ direction is because the decay instability condition dictates that $k^S \sim 2k^L \sim 2/\nu_{b,f}$.

[35] Figures 6 and 7 indicate that the product $n_{b,f}v_{b,f}$ (which defines the current associated to the beams) determines the angular spread associated with S waves off the beam direction. Recall that observation shows IAE to be largely field aligned with a small degree of angular spread about the parallel axis (15°) [*Foster et al.*, 1988; *Rietveld et al.*, 1991]. Note that the analysis of angular spread is not possible in 1-D approximation.

4. Discussion

[36] Let us now apply the results obtained thus far to explain observational data. First, consider the issue of plasma parameter g. The precise measurement of the plasma parameters inside IAE source regions is generally not available. Often, the only available measurement comes from adjacent regions of IAE source, which is characterized by turbulent density fluctuations. Therefore, substantial differences in the plasma parameters could be found between inside and outside the source region [*Forme and Fontaine*, 1999]. In view of this, a quantitative comparison between our theory and observation is not forthcoming as far as the influence of the plasma parameter is concerned, but we could nevertheless make a prediction that can be tested with future observation. Specifically, our findings show that S wave level increases for smaller values of g, where

$$g \propto n_e^{1/2}\, T_e^{-3/2}.$$

[37] The IAE characterized by long wavelength, or equivalently, $k \sim 0$, have not been adequately addressed in the literature by theoretical means, but their observation has been reported [*Foster et al.*, 1988; *Wahlund et al.*, 1992; *Forme et al.*, 1995]. *Dubois et al.* [1991] and *Guio and Forme* [2006] put forth theories based upon strong turbulence theory, but the present weak turbulent theory is able to offer an alternative explanation. Figures 4 and 5 show that $k \sim 0$ ion-acoustic modes are automatically generated during the decay instability, for a variety of beam densities and drift speeds. These enhancements at $k \sim 0$ are produced by decay instability, a feature revealed by analysis of the spontaneous decay term in (2), namely, $\propto I^{\sigma' L}_{\mathbf{k}'} I^{\sigma'' L}_{\mathbf{k}-\mathbf{k}'}$. Since this term must have a maximum for $I^{\sigma' L}_{\mathbf{k}'} I^{\sigma'' L}_{\mathbf{k}-\mathbf{k}'} \sim I^{\sigma' L}_{kd} I^{\sigma'' L}_{kd}$, where $k_d \sim 1/\nu_{b,f}$, it is seen that the S wave should be found for either $k \sim 2k' \sim 2k_d$ or $k \sim 0$. Induced decay terms are important only in later times, since these terms are $\propto I^{\sigma S}_{\mathbf{k}}$, while the L mode spectrum develops earlier.

[38] As mentioned already, field-aligned currents were proposed as the free energy source for IAE in the Earth's ionosphere. However, it was found that the threshold currents for the instability is too high in order to matching

Figure 6. Two-dimensional spectra for IAE when different beam densities are adopted. Here $\eta_b = \eta_f = 2$, $\tau = 5000$; $\eta_b = \eta_f = 6$, $\tau = 3000$; and $\eta_b = \eta_f = 10$, $\tau = 2000$ are shown. The beam speeds and the plasma parameter are $\eta_b = \eta_f = 5$ and $g = 10^{-6}$.

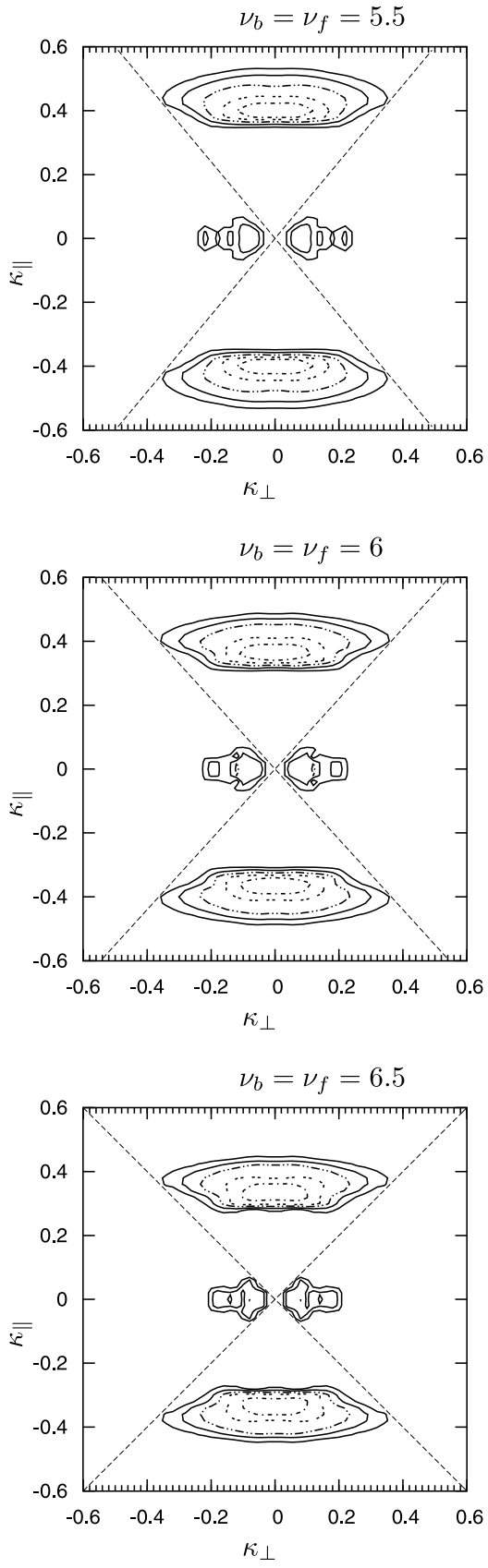

Figure 7. Two-dimensional spectra for IAE when different beam speeds are successively chosen. The beam densities and the plasma parameter are $\eta_b = \eta_f = 5$ and $g = 10^{-6}$ and $\tau = 2000$ in the three cases.

the observed levels of IAE [*Collis et al.*, 1991]. In this regard, the present counterstreaming beam model is particularly appealing, as such systems reduce the net current while maintaining the necessary free energy source for the instability to operate. The added advantage is that the counterstreaming beam system allows for a wider range of adjustable input parameters for a given value of the "beam current."

[39] Ion-acoustic enhancements in Earth's ionosphere are observed within a limited angular range $\lesssim 15°$ in relation to the geomagnetic field or field-aligned currents [*Foster et al.*, 1988; *Rietveld et al.*, 1991]. Figures 6 and 7 show that higher density for fixed drift speed leads to higher IAE levels as well as increasing the angular spread. Similarly, for fixed density, higher drift speed leads to wider angular spread. Comparing Figures 6 and 7 and observed angular spread, we may thus place a constraint on possible combinations of the beam density and drift speeds. In short, assuming that the present mechanism is indeed responsible for generating ionospheric IAE, one may deduce a set of physical parameters that characterizes the IAE source region.

[40] Another noteworthy point concerns ionospheric ion outflows. The present work considers stationary ion population, since IAE exhibit transient features and the ions dynamic evolves in a larger time scale. Considering that the ion-acoustic spectrum mainly develops along the beam (or geomagnetic field) direction, these ion-acoustic waves can be absorbed by ions, generating an energetic ion population, i.e., an ion flow, if the IAE are strong enough. It is true that ion outflows are often observed just before IAE [*Shulthess and St. Maurice*, 2001], but the above argument about the field-aligned characteristic of IAE allows one to suggest an increase in ion flows during IAE events for high enough levels of IAE. On the other hand, *Cabrit et al.* [1996] suggest that an overpopulation in the tail of the parallel ion velocity distribution could decrease the threshold for current-driven instability to enhance ion-acoustic waves. Therefore, ion outflows produced by IAE could act as a triggering mechanism for stream instability in upstream regions. Note that even symmetric IAE can produce ion outflows, since geomagnetic mirroring has the effect of aligning upgoing ions. This possibility concurs with the idea that Langmuir turbulence and stream instability may work together to produce the observed results [*Shulthess and St. Maurice*, 2001].

[41] Rayed aurora consists of a filamentary structure of bright auroral displays. IAE are also observed to display filamentary source structure during these events [*Grydeland et al.*, 2003; *Blixt et al.*, 2005]. Such filaments may well be the results of thin structures of up and downward current regions (hence, counterstreaming electron beams) in the ionosphere [*Neubert and Christiansen*, 2003].

[42] A single-beam model cannot explain why IAE are observed on the edges of precipitation structures rather than in the middle of an auroral ray [*Shulthess and St. Maurice*, 2001]. However, a counterstreaming model may account for

the observed phenomena. Assuming that filamentary bidirectional current structures are intermingled, the transition region *between* upgoing and down-going current regions must be characterized by counterstreaming electron beams. We have shown that IAE generation is greater in counterstreaming system than a single-beam system (Figure 4). This offers a natural explanation why IAE are preferentially generated on the edges of auroral rays.

[43] Figure 5 shows that ion-acoustic waves reach higher level for weak drift speeds. This is consistent with the observation that strong IAE result from low-energy electrons (low v_d), and that low-energy electron precipitation is usually related to IAE [*Collis et al.*, 1991; *Cabrit et al.*, 1996; *Blixt et al.*, 2005].

[44] Electron heating by a factor of ~2–3 or more is usually observed during IAE events while ion temperature remains nearly unchanged [*Rietveld et al.*, 1991; *Forme and Fontaine*, 1999]. While some degree of electron heating is observed in our numerical solutions, it is not enough to account for the observed electron heating.

[45] Finally, our model naturally can explain why sometimes IAE displays only a single spectral peak while at other times two simultaneous peaks are present. In fact, for sufficiently high beam density and plasma parameter g, we were able to obtain only one peak persisting in quasiasymptotic state. This occurred following the initial growth of near symmetrical peaks, which is followed by a strong damping of one peak [*Pavan et al.*, 2010]. It turns out that the upgoing (down-going) beam produces stronger down-going (upgoing) S waves. In the case of low-density beams, however, the results obtained in the present paper always feature down-going and upgoing peaks of S waves with similar amplitudes. However, the nonlinear dynamics of the beam-plasma instability has been shown to be strongly dependent on the parameters utilized [*Gaelzer et al.*, 2008]. Further investigations may be necessary to survey a wider range of parameters in order to investigate the possibility of formation of single IAE peaks in the case of low-density beams.

5. Conclusions

[46] To recap the major findings, the threshold current required for IAE generation is much lower for the counterstreaming beam system than a single beam system, which may thus account for the low current threshold during IAE events deduced from observation. IAE reach the highest intensity levels for symmetrical counterstreaming beams, which may account for a number of observed features including the fact that IAE events and rayed auroras are positively correlated.

[47] The present theory suggests that a theoretical constraint on the possible beam density and drift speed may be constructed on the basis of the theoretical angular spread and the observed value. Our theory also predicts that the background plasma ratio n_e/T_e is to play an important role with regards to S waves intensity. It was found that the smaller the ratio n_e/T_e the stronger the S wave enhancement. Such a prediction can be tested by future observation.

[48] The present paper also suggests ion flow increase by strong IAE since the enhancements develop mainly along the beam direction. In addition, within our model, an expected consistency relating IAE and auroral activity is found since auroral events involve field-aligned currents in ionosphere.

[49] Finally, a study exploring other parameters may be in order, specially aiming to obtainment of IAE spectra featuring one peak only. These items may constitute a future work.

[50] **Acknowledgments.** This work was partially supported by the Brazilian agencies CNPq and FAPERGS. P.H.Y. acknowledges support by AFOSR contract FA9550070053 to MTL, NSF grant ATM0836364 to the University of Maryland, and the Korean Ministry of Education, Science and Technology under WCU grant R31-10016 to KHU.

[51] Amitava Bhattacharjee thanks the reviewers for their assistance in evaluating this paper.

References

Blixt, E. M., T. Grydeland, N. Ivchenko, T. Hagfors, C. La Hoz, B. S. Lanchester, U. P. Løvhaug, and T. S. Trondsen (2005), Dynamic rayed aurora and enhanced ion-acoustic radar echoes, *Ann. Geophys.*, *23*, 3.

Block, L. P., and C. G. Fälthammar (1990), The role of magnetic-field-aligned electric fields in auroral acceleration, *J. Geophys. Res.*, *95*, 5877.

Buchert, S. C., A. P. van Eyken, T. Ogawa, and S. Watanabe (1999), Naturally enhanced ion-acoustic lines seen with the EISCAT Svalbard radar, *Adv. Space Res.*, *23*, 1699.

Burke, W. J., M. Silevitch, and D. A. Hardy (1983), Observations of small scale auroral vortices by the S3-2 satellite, *J. Geophys. Res.*, *88*, 3127.

Bythrow, P. F., T. A. Potemra, W. B. Hanson, L. J. Zanetti, C.-I. Meng, R. E. Huffman, F. J. Rich, and D. A. Hardy (1984), Earthward directed high-density Birkeland currents observed by HILAT, *J. Geophys. Res.*, *89*, 9114.

Cabrit, B., H. Opgenoorth, and W. Kofman (1996), Comparison between EISCAT UHF and VHF backscattering, *J. Geophys. Res.*, *101*, 2369.

Collis, P. N., I. Häggström, K. Kaila, and M. T. Rietveld (1991), EISCAT radar observations of enhanced incoherent scatter spectra: Their relation to red aurora and field-aligned currents, *Geophys. Res. Lett.*, *18*, 1031.

DuBois, D. F., H. A. Rose, and D. Russell (1991), Coexistence of parametric decay cascades and caviton collapse at subcritical densities, *Phys. Rev. Lett.*, *66*, 1970.

Edney, S. D., and P. A. Robinson (2001), Analytical treatment of weak-turbulence Langmuir wave electrostatic decay, *Phys. Plasmas*, *8*, 428.

Forme, F. R. E. (1993), A new interpretation of the origin of enhanced ion acoustic fluctuations in the upper ionosphere, *Geophys. Res. Lett.*, *20*, 2347.

Forme, F. R. E. (1999), Parametric decay of beam-driven Langmuir wave and enhanced ion-acoustic fluctuations in the ionosphere: A weak turbulence approach, *Ann. Geophys.*, *17*, 1171.

Forme, F. R. E., and D. Fontaine (1999), Enhanced ion acoustic fluctuations and ion outflows, *Ann. Geophys.*, *17*, 182.

Forme, F. R. E., D. Fontaine, and J. E. Wahlund (1995), Two different types of enhanced ion acoustic fluctuations observed in the upper ionosphere, *J. Geophys. Res.*, *100*, 14,625.

Foster, J. C., C. del Pozo, K. Groves, and J.-P. St. Maurice (1988), Radar observations of the onset of current driven instabilities in the topside ionosphere, *Geophys. Res. Lett.*, *15*, 160.

Gaelzer, R., L. F. Ziebell, A. F. Viñas, P. H. Yoon, and C.-M. Ryu (2008), Asymmetric solar wind electron superthermal distributions, *Astrophys. J.*, *677*, 676.

Grydeland, T., C. La Hoz, T. Hagfors, E. M. Blixt, S. Saito, A. Strømme, and A. Brekke (2003), Interferometric observations of filamentary structures associated with plasma instability in the auroral ionosphere, *Geophys. Res. Lett.*, *30*(6), 1338, doi:10.1029/2002GL016362.

Guio, P., and F. R. E. Forme (2006), Zakharov simulations of Langmuir turbulence: Effects on the ion-acoustic waves in incoherent scattering, *Phys. Plasmas*, *13*, 122,902.

Kontar, E. P., and H. L. Pécseli (2005), Nonlinear wave interactions as a model for naturally enhanced ion acoustic lines in the ionosphere, *Geophys. Res. Lett.*, *32*, L05110, doi:10.1029/2004GL022182.

McFadden, J. P., C. W. Carlson, and R. E. Ergun (1999), Microstructure of the auroral acceleration region as observed by FAST, *J. Geophys. Res.*, *104*, 14,453.

Neubert, T., and F. Christiansen (2003), Small-scale, field-aligned currents at the top-side ionosphere, *Geophys. Res. Lett.*, *30*(19), 2010, doi:10.1029/2003GL017808.

Pavan, J., L. F. Ziebell, P. H. Yoon, and R. Gaelzer (2009), Decay of beam-driven Langmuir wave into ion-acoustic turbulence in two dimensions, *Plasma Phys. Controlled Fusion*, *51*, 095011.

Pavan, J., L. F. Ziebell, P. H. Yoon, and R. Gaelzer (2010), Generation of quasi-isotropic electron population during nonlinear beam-plasma interaction, *J. Geophys. Res.*, *115*, A01103, doi:10.1029/2009JA014447.

Rietveld, M. T., P. N. Collis, and J.-P. St. Maurice (1991), Naturally enhanced ion acoustic waves in the auroral ionosphere observed with the EISCAT 933-MHz radar, *J. Geophys. Res.*, *96*, 19,291.

Shulthess, F. S., and J.-P. St. Maurice (2001), Naturally enhanced ion-acoustic spectra and their interpretation, *Surv. Geophys.*, *22*, 55.

Wahlund, J.-E., F. R. E. Forme, H. J. Opgenoorth, M. A. L. Persson, E. V. Mishin, and A. S. Volokitin (1992), Scattering of electromagnetic waves from a plasma: Enhanced ion acoustic fluctuations due to ion-ion two-stream instabilities, *Geophys. Res. Lett.*, *19*, 1919.

Yoon, P. H., T. Rhee, and C.-M. Ryu (2006), Self-consistent formation of electron κ distribution: 1. Theory, *J. Geophys. Res.*, *111*, A09106, doi:10.1029/2006JA011681.

Ziebell, L. F., R. Gaelzer, J. Pavan, and P. H. Yoon (2008), Two-dimensional nonlinear dynamics of beam-plasma instability, *Plasma Phys. Controlled Fusion*, *50*, 085011.

R. Gaelzer, Instituto de Física e Matemática, Universidade Federal de Pelotas, 96010-900 Pelotas, Brazil. (rudi@ufpel.edu.br)

J. Pavan and L. F. Ziebell, Instituto de Física, Universidade Federal do Rio Grande do Sul, 91501-970 Porto Alegre, Brazil. (joel.pavan@ufrgs.br; ziebell@if.ufrgs.br)

P. H. Yoon, Institute for Physical Science and Technology, University of Maryland College Park, College Park, MD 20742, USA. (yoonp@umd.edu)